ELSEVIER

Contents lists available at ScienceDirect

Deep-Sea Research Part I

journal homepage: www.elsevier.com/locate/dsri



Phytoplankton growth and grazing dynamics during anomalous heat wave and suppressed upwelling conditions in the southern California Current

Michael R. Landry a,* , Alexandra L. Freibott a , Michael R. Stukel b , Karen E. Selph c , Andrew E. Allen a,d , Ariel Rabines a,d

ARTICLE INFO

Keywords: Growth Grazing mortality Dilution Prochlorococcus Synechococcus Picoeukaryotes California current ecosystem

ABSTRACT

We investigated phytoplankton dynamics in the southern California Current System (SCCS) in August 2014 during the early phase of the 2014-15 marine heat wave (MHW). Multi-day experiments were conducted at three inshore and two offshore sites, with daily depth profiles of dilution incubations on a drifting array to determine growth and grazing rates and shipboard assessments of nutrient effects. Picophytoplankton populations were analyzed by flow cytometry and eukaryotic phytoplankton by 18 S sequencing. Mixed-layer nutrients were low across the region, but inshore sites had substantial nitrate concentrations and prominent Chla maxima in the lower euphotic zone. Shoreward transport of warm-stratified waters from the offshore suppressed coastal upwelling and shifted picophytoplankton distributions toward increased onshore abundance of Prochlorococcus and decreased Synechococcus and picoeukaryotes. These trends were reinforced by higher-than-average growth of Prochlorococcus at inshore sites and higher grazing of Synechococcus and picoeukaryotes. Prasinophytes (Chlorophyceae) were notably important among eukaryotic taxa, and pennates replaced centric taxa as the dominant diatoms in inshore waters compared to normal upwelling. Despite substantial spatial variability in community composition, offshore and inshore experimental locations both showed growth-grazing balances, with microzooplankton consuming similar percentages (80%) of primary production. We thus confirm expectations that the 2014-15 MHW resulted in greater trophic flow through the microbial food web at the expense of reduced direct phytoplankton (Chla) consumption by mesozooplankton. However, impacts on mesozooplankton energy budgets were partially offset by increased trophic flow through protistan microzooplankton and higher phytoplankton C: Chla.

1. Introduction

Marine Heatwaves (MHW) are recurrent natural perturbations of the marine environment that are predicted to intensify in frequency and magnitude with ocean warming (Di Lorenzo and Mantua, 2016; Frölicher and Laufkötter, 2018). In the northeastern Pacific, the largest MHW on record began in winter 2013–14 as an atmospheric forcing event in the Gulf of Alaska associated with the North Pacific Oscillation (NPO) and was extended through early 2016 by ocean teleconnections and feedbacks that initiated El Niño conditions and a positive (warm phase) shift of the Pacific Decadal Oscillation (PDO) (Di Lorenzo and Mantua, 2016; Xu et al., 2021). Numerous reports have emphasized the

northern origin of the 2014-15 MHW and its various impacts on higher trophic level populations, including seabirds, marine mammals and shellfish fisheries (Bond et al., 2015; Kintish, 2015; Leising et al., 2015; Peterson et al., 2015; McCabe et al., 2016; McClatchie et al., 2016; Peña et al., 2019; Shanks et al., 2020). Over the California Current region as a whole, however, average 2014–15 anomalies of phytoplankton biomass (Chla) and production were more strongly negative and longer lasting in the southern sector (23–32°N) off Southern California and Baja Mexico than in the north (35–48°N) (Gómez-Ocampo et al., 2017).

Off Southern California, seawater temperatures during the 2014-15 MHW reached 4–5 $^{\circ}$ C above seasonal averages for the upper 50 m (Zaba and Rudnick, 2016), with 2-year averaged mixed layer anomalies

E-mail address: mlandry@ucsd.edu (M.R. Landry).

https://doi.org/10.1016/j.dsr.2024.104353

^a Scripps Institution of Oceanography, University of California at San Diego, La Jolla, CA, 92093-0227, USA

^b Earth, Ocean, and Atmospheric Science Department, Florida State University, Tallahassee, FL, 32306, USA

^c Department of Oceanography, University of Hawai'i at Manoa, Honolulu, HI, 96822, USA

^d Microbial and Environmental Genomics, J. Craig Venter Institute, La Jolla, CA, USA

^{*} Corresponding author.

of +2 °C extending almost uniformly to 700-km seaward (Landry et al., 2024). Stratification was further strengthened by a subsurface salinity minimum at ~90 m (Zaba and Rudnick, 2016). Ocean fronts, typically sites of enhanced vertical exchange and productivity, declined in frequency and magnitude (Kahru et al., 2018), and nitracline depths were 14-24 m deeper than the previous 9-year average (Landry et al., 2024). Documented impacts on the pelagic community include a 2-3 fold decrease in mixed-layer Chla and a significant increase in picophytoplankton contribution to phytoplankton carbon biomass, led principally by higher Prochlorococcus abundance in inshore waters (Landry et al., 2024). In contrast, Synechococcus and picoeukaryotes declined generally across the system and especially in the offshore. Rates of mesozooplankton grazing and egg production were low compared to normal conditions but followed similar functional relationships relative to ambient Chla biomass (Morrow et al., 2018; Nickels and Ohman, 2018). Notably missing in the understanding of these lower food web responses are the intermediate processes (phytoplankton growth and microzooplankton grazing) that might explain differences in population abundance trajectories and indirect mesozooplankton connections to primary production.

Process cruise P1408 was conducted by the CCE-LTER (California Current Ecosystem, Long-Term Ecological Research) Program in August 2014 when anomalous ocean conditions with severely reduced winds and upwelling, surface water warming and reduced chlorophyll a (Chla) were observed to be occurring from Oregon to southern California but not yet linked to a specific forcing mechanism. Anticipating at the time that it might be a short-term event, the P1408 science plan was adapted to investigate the normally dynamic upwelling region off Point Conception, laying the groundwork to document upwelling resurgence later in the cruise. In retrospect, anomalies in mixed-layer temperature, nitrate concentration and nitracline depth for the upwelling region in August 2014 had not yet reached seasonal mean values for the full 2014-15 period (Landry et al., 2024). We thus characterize P1408 as capturing the 2014-15 MHW when physical features of the warming perturbation were still building in the Southern California Current System (SCCS) and use cruise results to evaluate lower food web responses during the early phase of this major ocean warming event (Fig. 1).

Increased energy flow through protistan microzooplankton and more balanced growth and loss processes (system recycling rather than biomass accumulation) are expected consequences of a future warmer, more-stratified ocean where small phytoplankton dominate (Bopp et al., 2013; Flombaum et al., 2020). Here, we evaluate these hypotheses using

measured rates of growth and microzooplankton grazing for different components of the phytoplankton community (*Prochlorococcus*, *Synechococcus*, picoeukaryotes, total Chla) in August 2014 and in comparison to similarly measured rates during normal upwelling conditions. Additional study features – including *in situ* incubations on free drifting arrays, experiments with and without added nutrients, and 18 S sequence analyses – provide insights into the relationships of physical circulation, nutrient effects and net ambient community growth rates to onshore and offshore distributional patterns, as well as compositional differences in eukaryotic phytoplankton between heat wave and normal upwelling conditions.

2. Materials and methods

2.1. Sampling and experimental set-up

Cruise P1408 was conducted on *R/V Melville* from 6 August to September 5, 2014 off of Point Conception, California. Following the standard quasi-Lagrangian design of CCE Process cruises (Landry et al., 2009), sampling and experiments were done as "cycles" of repeated daily activities following the advective transport of a satellite-tracked drift array that also served as the platform for *in situ* bottle incubations. For P1408, we conducted five experimental cycles (C1–C5), each of three-day duration beginning with a hydrocast at the start of day 1 and ending with a fourth time-point hydrocast at the end of day 3 (Fig. 1A). Fig. 1B shows the progression of temperature anomalies off California from December 2013 cool conditions to warming SST preceding the P1408 cruise and sustained warm conditions for a year after the cruise.

Water samples for standing stock and rate determinations were collected in Niskin bottles from CTD hydrocasts (02:00 local time) in close proximity (\sim 100 m) to the drifter. Specific sampling depths, ranging from 2 to 120 m, were adjusted to the Chla profiles of each cycle experiment. To assess the lower depth distributions of Chla and picophytoplankton populations, we sampled 8 depths extending below the deep fluorescence maximum. Experimental incubations were conducted with water from the upper 6 depths, which captured the euphotic zone defined by the depth of penetration of 1% of incident Photosynthetically Available Radiation (PAR), assessed on daily noon hydrocasts. Samples for initial Chla measurements (250 mL) and molecular analyses (300–500 mL) were filled directly from the CTD Niskin bottles. Samples (50 mL) for macronutrient concentrations were filtered through a 0.1-µm capsule filter (Suporcap) and frozen (-20 °C) for later laboratory

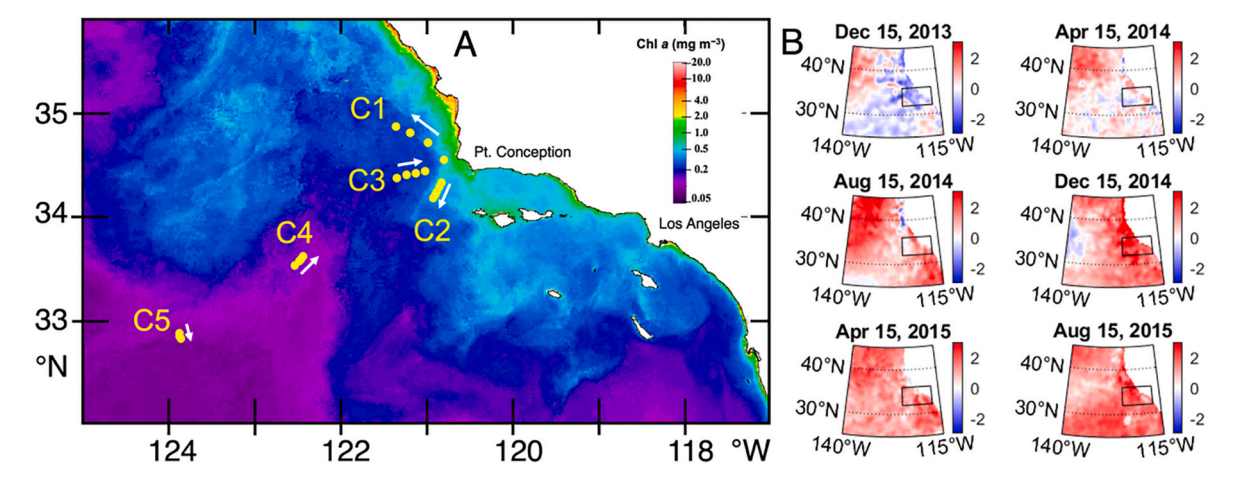


Fig. 1. A) Sampling locations during CCE Process cruise P1408. C1–C5 are the sites of daily CTD casts for experimental Cycles 1–5 following a satellite-tracked drifter. Arrows denote the direction of drifter transport. Chla is the merged ocean color product from MERIS, MODIS-Aqua and MODIS-Terra data for August 2014 (courtesy M. Kahru). B) Sea-surface temperature anomalies (°C) off California from December 2013 to August 2016 from the AVHRR optimally interpolated satellite dataset with 0.25° spatial resolution (https://podaac.jpl.nasa.gov/dataset/AVHRR_OI-NCEI-L4-GLOB-v2.0). Anomaly is calculated relative to 1982–2021 climatology. Black rectangle is the study region in A. Aug. 15, 2014 matches the approximate midpoint of cruise P1408.

analysis by autoanalyzer.

For each experimental depth, we prepared a two-treatment dilution experiment (Landry et al., 2008, 2011), with one polycarbonate bottle (2.7 L) containing unfiltered seawater (100%) and the second (diluted) bottle consisting of \sim 33% whole seawater with filtered water from the same depth. Seawater was filtered directly from the Niskin bottles using a peristaltic pump, silicone tubing and in-line 0.1-µm Suporcap filter capsules that had previously been acid washed. Dilution bottles were first given a measured volume of filtered water and then filled gently to the top with unscreened water from the Niskin bottles to avoid physical damage to fragile protists. Nutrients were not added to incubation bottles to minimize impacts on grazing rates in oligotrophic waters (Lessard and Murrell, 1998). Each filled bottle was subsampled for flow cytometry (FCM) analysis (1-2 mL) of picophytoplankton concentrations. The bottles were then placed in coarse net bags and attached to the line below the drifter float at the depth of collection and incubated in situ for 24 h.

All array deployments were completed pre-sunrise. For deployments on successive days within an experimental cycle, we collected water adjacent to the array and set up the second set of experiments before recovering the first. Switching of net bags and redeployment were generally done within 10 min while the ship maintained position. Upon array recovery, each bottle was subsampled for final Chla concentrations and picophytoplankton cell abundances.

During each cycle, we also prepared one traditional multi-treatment dilution experiment (Landry and Hassett, 1982) using mixed-layer water (10 m) from an evening hydrocast in the same water parcel sampled for the two-treatment incubations. Replicated dilution treatments of 0.22, 0.45, 0.65, 0.86 and 1.0 X natural seawater were prepared in 2.2-L polycarbonate bottles as above, by first adding measured aliquots of filtered water. Each dilution treatment bottle received added nutrients (final concentrations of 5 μM nitrate, 0.5 μM phosphate) to promote constant phytoplankton growth. Two additional bottles were also prepared as controls without added nutrients. Each bottle was then filled with natural unscreened seawater from the depth of collection, via a mixing carboy that was filled gently via submerged tubing from several rosette bottles. All bottles were incubated for 24 h in a seawater cooled incubator screened to 31% of surface irradiance. We sampled each dilution bottle initially and at 24 h for flow cytometry. Triplicate initial Chl a samples (250 mL) were taken from the mixing carboy, and initial Chl a estimates in dilution bottles were computed volumetrically from the proportions of filtered and unfiltered water added. Final Chl a samples were taken from each experimental bottle.

2.2. Flow cytometry and chlorophyll analyses

Population abundances of picophytoplankton (Prochlorococcus, Synechococcus and phototrophic pico-eukaryotes) were determined from 1 mL FCM samples, which were preserved (0.5% paraformaldehyde, v/v, final concentration) frozen in liquid nitrogen on the ship, and stored at −80 °C until analysis. Thawed samples were stained with Hoechst 33342 (1 μg mL⁻¹, v/v, final concentration) at room temperature in the dark for 1 h (Monger and Landry, 1993). Aliquots (100 µL) were analyzed using a Beckman-Coulter EPICS Altra flow cytometer with a Harvard Apparatus syringe pump for volumetric sample delivery and co-linear excitation by two water-cooled argon ion lasers tuned to 488 nm (1 W) and the UV range (200 mW) (Selph et al., 2011, 2016). The optical filter configuration distinguished populations on the basis of chlorophyll a (red fluorescence, 680 nm), phycoerythrin (orange fluorescence, 575 nm), DNA (blue fluorescence, 450 nm), and forward and 90° light scatter signatures. Calibration beads (0.5 μm yellow-green beads and UV beads) were used as fluorescence standards. Raw data (listmode files) were processed using the software FlowJo (Treestar Inc., www.flowjo.com).

Samples (250 ml seawater) for initial and final concentrations of chlorophyll a (Chl a) were filtered onto 25-mm Gelman GF/F filters,

extracted in 7 ml of 90% acetone at $-20~^{\circ}\text{C}$ for 24 h and analyzed on shipboard with a calibrated Turner 10AU fluorometer according to the standard procedures of the California Cooperative Oceanic and Fisheries Investigations (CalCOFI, http://calcofi.org/references/methods/8-chlorophyll-methods.html).

2.3. Molecular analyses

Community compositions were analyzed by 18 S molecular sequencing for a subset of samples to assess onshore-offshore taxonomic variability during P1408 and to compare to taxa from inshore locations sampled during strong upwelling conditions on two previous cruises. Each of the five P1408 cycle experiments was sampled 5–9 times, typically at 12 and 25 m but extending to 40 m for offshore sites with deeper euphotic zones. Comparative analyses from previous cruises (4 samples each from P0605 in May 2006 and P0704 in April 2007) were taken close to the starting locations for C1 and C2 in Fig. 1.

Samples for molecular analyses were filtered onto 0.2-µm Supor filters, flash frozen in liquid nitrogen, and stored at $-80\,^{\circ}\text{C}$ until analysis. Filtered samples were extracted using the NucleoMag 96 Plant kit and amplified using polymerase chain reaction (PCR). Eukaryotes were amplified by targeting 18 S rDNA in the hypervariable V9 (1389 F-TTGTACACACCGCCC, 1510 R-CCTTCYGCAGGTTCACCTAC) and V4 (F-CCAGCASCYGCGGTAATTCC, R-ACTTTCGTTCTTGATYR) regions. Amplified DNA was purified using the AMPure XP kit and samples were pooled at ≤ 1 ng DNA concentrations before sequencing on an Illumina MiSeq.

Paired sequencing reads from 18 S V9 amplicons were quality trimmed to Phred score 30 (Q30, minimum average, in sliding window of size 2 bp). Paired reads were aligned using PEAR (Zhang et al., 2014) and then filtered to remove possible chimeras using USEARCH (Edgar, 2010) and a minimum length of 50 bp. Paired reads from 18 S V4 were quality trimmed to Q20 due to the lower maximum quality scores of these sequences, but only read 1 was used due to the poor quality of read 2. Quality control resulted in a total of 523,266 reads (mean 47,569 \pm 22,207 per sample) for 18 S V9 samples and 217,777 reads (21,777 mean \pm 7243 per sample) for 18 S V4 samples. Metazoan sequences were removed from both 18 S datasets, leaving a total of 89,324 (mean 14,887 \pm 5857 per sample) in the V9 dataset and 199,337 (19,933 \pm 5806 per sample) in the V4 dataset.

Reads were clustered into operational taxonomic units (OTUs) using SWARM (Mahé et al., 2014), and custom python scripts were used to aggregate library specific OTU read counts (https://github.com/allenlab/rRNA_pipeline). Using the PR2 database with taxonomic updates from the Tara Oceans W2 (de Vargas et al., 2015), a total of 3685 OTUS were identified in the V9 samples and 5574 in the V4 samples.

2.4. Environmental variables

Environmental variables were determined from products available at the data repository for CCE cruises at https://oceaninformatics.ucsd.edu/datazoo/catalogs/ccelter/datasets. Profiles of temperature, salinity and nutrients are measurements from the bottle trip depths of the hydrocasts from which experimental water was collected. Mixed-layer depth (MLD), defined as the depth at which sigma-t density first exceeds surface values by 0.01 kg m $^{-3}$, was determined from the calculated density profile of CTD downcast files at 1-m resolution. Nitracline is the depth at which NO $_3$ concentration first exceeds 1.0 μ M. Incident Photosynthetically Available Radiation at the sea surface (PAR $_0$) was determined by integrating continuous measurements of the ship's PAR sensor (2.5-min resolution) for the daylight hours of each incubation day. Euphotic Zone (EZ $_{1\%}$), the depth of penetration of 1% of PAR $_0$, was computed from mean light extinction coefficients determined from PAR sensors on CTD hydrocasts around local noon of each day.

2.5. Rate estimates from dilution experiments

From the two-treatment dilution experiments, we determined profiles for instantaneous growth rate $(\mu_0,\,d^{-1}),$ grazing mortality $(m,\,d^{-1})$ and net growth rate $(k,\,d^{-1})$ from each pair of incubated bottles and for each parameter measured (Chl a, FCM populations) according to equations in Landry et al. (1984, 2008). Estimates of k come directly from incubation bottles containing undiluted seawater; k=1/t * ln $(P_f/P_o),$ where t=1 day and P_o and P_f are initial and final measurements of population abundances. Estimates of m are determined from the difference in net growth rates in the diluted $(k_d,\,d^{-1})$ and undiluted treatments, where D is the dilution factor (proportion of natural seawater in the diluted treatment; $m=(k_d-k)/(1-D)$. Estimates of μ are the sum of net growth and grazing loss $(\mu=k+m)$.

For the multi-treatment dilution experiments, we computed daily growth and grazing rates by the standard linear regression and control treatment approach (Landry and Hassett, 1982; Landry et al., 1998). Growth rates with added nutrients (μ_n , intercept) and m (slope) were determined from the regression $k_n=\mu_n$ - (D * m), where $k_n=$ the measured net growth rate in each bottle of the dilution series with added nutrients and D is the proportion of unfiltered seawater in the treatment. Ambient growth rate estimates without added nutrients (μ_0) are then determined by adding grazing estimates to the net growth rates (k) measured in bottles without added nutrients, $\mu_0=k+m$. Differences, if any, between μ_n and μ_0 are taken to be indicative of possible nutrient limitation effects (Landry et al., 1998).

2.6. Net growth rates in the ambient water column

Net growth rates of Chla and picophytoplankton populations in the ambient environment were determined from the changes in water-column samples collected on successive days following the experimental drifter. For each experiment day, we integrated the concentration profiles for the initial experimental hydrocast (C_0) and the hydrocast taken 24-h (C_{24}) later when the array incubation experiments were retrieved. Daily net growth rates were computed as $ln (C_{24}/C_0)$. Cycle-average net growth rates are the mean values $(\pm SEM)$ for the three days of cycle duration, corresponding to the same days of in situ bottle incubations on the drift array.

3. Results

3.1. Study sites and environmental conditions

Three of the P1408 cycle experiments (C1–C3) were initiated at coastal sites typically characterized by high nutrients and phytoplankton blooms due to upwelling (Fig. 1). The array deployed for experiment C1 began closest to Point Conception and drifted strongly to the northwest over 3 days. C2 was initiated south of C1 and moved to the southwest. C3 began offshore and between the ending locations of C1 and C2 and was advected eastward toward Point Conception. Offshore experiment C4 was located in a tongue of low-Chla surface water

moving northeastward toward the coast. C5 was furthest offshore in an area of very slow southward drift.

All cycle sites were strongly stratified with shallow mixed layers (10-24 m) and low mixed-layer concentrations of dissolved nitrate (0.04-0.07 µM NO₃) (Table 1). Euphotic zone (EZ) depths varied from 31 to 44 m for inshore cycles C1-C3 and 64-77 m for the offshore cycles C4–C5. Nitracline depths ranged from 25 to 35 m for the inshore cycles and 69–89 m in the offshore. Inshore cycles thus differed by the presence of substantial nitrate concentrations in the lower EZ and prominent deep Chla maxima (DCMs) at those sites, while the nitraclines at offshore sites resided below EZ1% and DCMs were muted (Fig. 2C and D). Hydrographically, C1 and C2 separate cleanly from C4 and C5 with the inshore sites being 3–4 $^{\circ}$ C cooler and 0.4–0.5 ps μ more saline throughout the EZ depth strata compared to the offshore waters (Fig. 2A and B). In contrast, the profiles for C3 suggest mixed influences, with temperature and Chla being more similar to C4–C5 than to C1–C2 inshore sites in the upper EZ (<20 m) and salinity being more similar to C4-C5 in the lower EZ (Fig. 2A and B).

3.2. Picophytoplankton abundances and depth distributions

Mean EZ abundances of *Prochlorococcus* were highest and similar at offshore sites (157 \pm 12 versus $158 \pm 27 \times 10^3$ cells mL $^{-1}$ for C4 and C5, respectively), lowest for C1 (10 \pm 2 \times 10 3 cells mL $^{-1}$), and intermediate for other inshore sites C2 and C3 (77 \pm 11 and 120 \pm 23 \times 10 3 cells mL $^{-1}$, respectively) (Fig. 3A). While depth distributions for most cycles were fairly uniform, on average, before declining sharply at the EZ base, *Prochlorococcus* densities for C3 were similar to those for C4 and C5 in the mixed layer and more like the profile for C2 below 20 m.

Synechococcus abundances were lowest for the offshore experiments (4.8 \pm 0.1 and 3.1 \pm 0.8 \times 10^3 cells mL^{-1} for C4 and C5), highest for C2 (95 \pm 4 \times 10^3 cells mL^{-1}), and intermediate for C1 and C3 (45 \pm 10 and 64 \pm 8 \times 10^3 cells mL^{-1} , respectively) (Fig. 3B). Depth distributions were relatively uniform, on average, throughout the EZ for C2, C3 and C5. However, deep maxima (2–4 times surface densities) were evident in the lower EZ (40–60 m) for all C4 profiles, and Synechococcus declined abruptly in the depth range of the Chla maxima in all C1 profiles.

Mean EZ abundances for picoeukaryotes were also lowest for the offshore experiments (4.8 \pm 0.5 and 2.5 \pm 0.3 \times 10 3 cells mL $^{-1}$ for C4 and C5) but similar overall for the inshore cycles (11.2 \pm 0.7, 12.4 \pm 0.7 and 13.2 \pm 0.6 \times 10 3 cells mL $^{-1}$ for C1–C3, respectively) (Fig. 3C). In contrast to *Prochlorococcus* and *Synechococcus*, picoeukaryotes typically exhibited abundance maxima in the deep EZ, with the exception of a sharp picoeukaryote decline, similar to *Synechococcus* abundance, in the DCM depth range for C1 (Fig. 3B and C).

3.3. Growth and grazing estimates from in situ incubations

Chla-based estimates of phytoplankton growth and grazing rates range between maximal mean values of $0.6\ d^{-1}$ in the upper to not significantly different from zero in the lower EZ (Fig. 4A and B). Growth rate maxima are $0.5\ d^{-1}$ or higher for all cycles except C1 (max = 0.3

Table 1 Start dates, locations and environmental conditions for phytoplankton incubations during P1408 Cycle 1–5 experiments in August 2014. Mixed-layer depth (MLD) is the depth where sigma-t density exceeds surface values by 0.01 kg m^{-3} . PAR₀ is incident photosynthetically available radiation at the sea surface. Temp_{ML} and NO3_{ML} are mean mixed-layer temperature and nitrate concentrations, respectively. Nitracline is the depth at which NO₃ concentration first exceeds 1.0μ M. Euphotic Zone (EZ_{1%}) is the depth of penetration of 1% of PAR₀. Uncertainties are standard errors of mean values for three days of experimental incubations.

Cycle	Start	Lat	Long	MLD	$Temp_{ML}$	NO3 _{ML}	PAR ₀	Nitracline	EZ _{1%}
	Date	(°N)	(°W)	(m)	(°C)	(μΜ)	(Ei $m^{-2} d^{-1}$)	(m)	(m)
C1	11 Aug	34.51	120.77	11.3 ± 4.7	16.4 ± 0.08	0.06 ± 0.02	69.1 ± 2.6	24.7 ± 0.3	31.4 ± 0.6
C2	17 Aug	34.27	120.82	24.3 ± 0.3	16.8 ± 0.06	0.07 ± 0.01	58.2 ± 9.4	35.3 ± 0.3	40.4 ± 0.2
C3	22 Aug	34.39	121.39	10.0 ± 1.7	18.5 ± 0.12	0.04 ± 0.01	61.0 ± 1.5	25.3 ± 0.3	43.9 ± 1.4
C4	26 Aug	33.52	122.56	12.0 ± 1.7	19.2 ± 0.06	0.04 ± 0.01	67.8 ± 11.3	68.7 ± 0.3	64.2 ± 3.1
C5	30 Aug	32.88	123.90	22.3 ± 4.9	19.8 ± 0.01	0.04 ± 0.01	83.8 ± 0.4	88.7 ± 0.3	76.6 ± 4.5

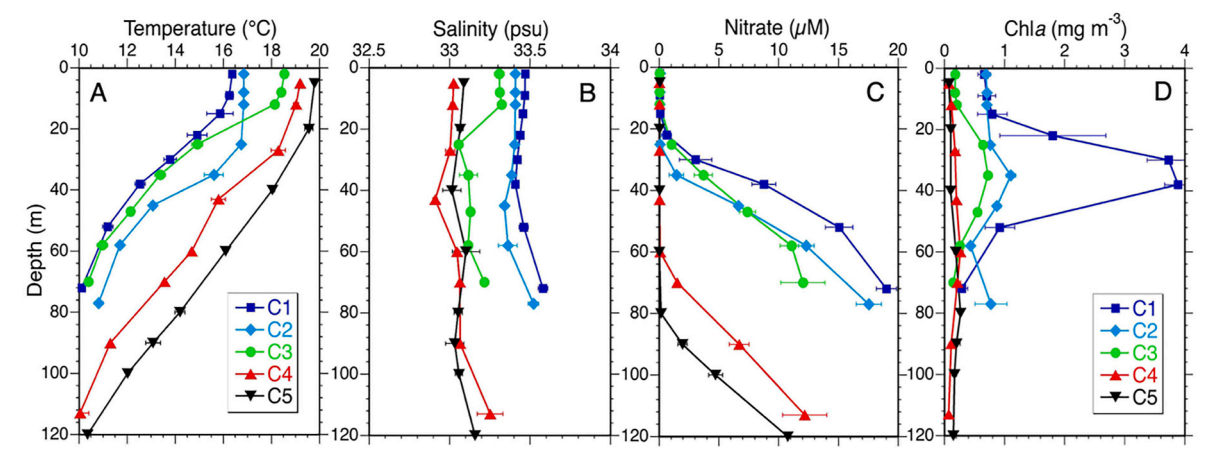


Fig. 2. Mean profiles of temperature, salinity, nitrate and chlorophyll *a* from CTD casts that initiate incubation experiments during Cycles 1–5. Uncertainties are standard errors of mean values.

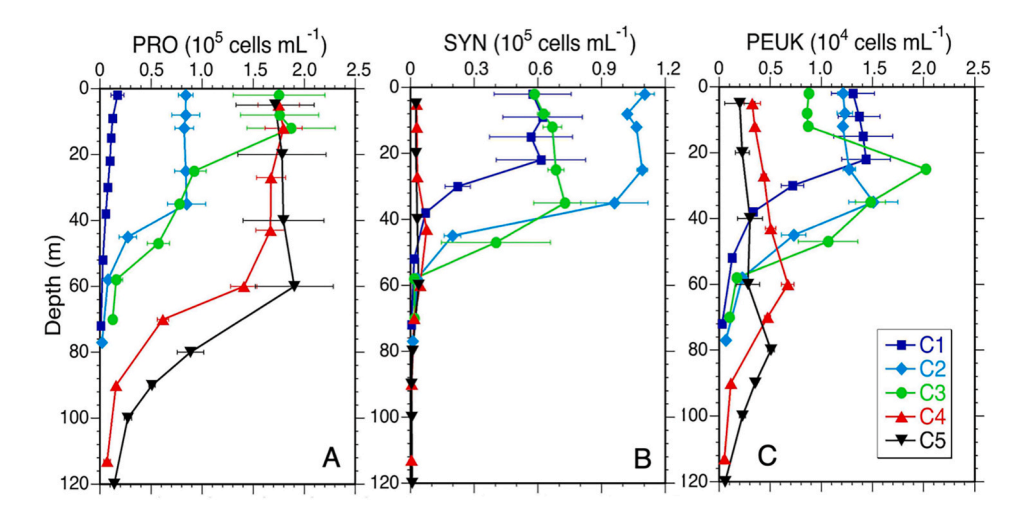


Fig. 3. Mean depth profiles of cell abundances for picophytoplankton populations during Cycles 1–5. PRO = Prochlorococcus; SYN = Synechococcus; PEUK = picoeukaryotes. Uncertainties are standard errors of mean values.

 d^{-1}). All cycles have primary (C1–C2, C4–C5) or secondary (C4) growth maxima in subsurface waters, but shallower than the DCM or picoeukaryote abundance maxima (Fig. 3C and 4A). Grazing rate estimates are typically similar to growth, on average, but with different depth distributions, such that C1 and C2 show excess grazing and negative net growth rates in the upper 10 m, while C3 and C4 have mixed-layer grazing deficits and positive net growth in that stratum (Fig. 4B). Except for C2, all profiles show subsurface maxima in net growth rates $(0.1–0.3\ d^{-1})$ between 20 and 40 m (Fig. 4C).

Taxon-specific growth and grazing rate estimates from the *in situ* incubations range up to $1.8~{\rm d}^{-1}$ for *Prochlorococcus* and $2.1~{\rm d}^{-1}$ for *Synechococcus* and picoeukaryotes, with maxima in the upper 20 m (Fig. 4). For *Prochlorococcus*, growth rates are highest for C1 and C2 and exceed grazing estimates in the mixed layer for all inshore stations, leading to positive net growth in the upper $12~{\rm m}~(0.2-0.9~{\rm d}^{-1})$ for cycles C1–C3 (Fig. 4D–F). Grazing exceeds growth below 20 m for C1 and C2, giving a sharp transition to net negative growth in the DCM for those cycles, while net growth in the DCM is close to zero for C3. Compared to the inshore sites, growth and grazing estimates for the offshore cycles strongly covary over the full EZ such that net growth rates are uniformly zero (C4) or slightly negative (C5) (Fig. 4F).

In contrast to the growth rate maxima for *Prochlorococcus* for inshore cycles, the highest values for *Synechococcus* and picoeukaryotes are for offshore cycles C4 and C5, respectively (Fig. 4G–J). For *Synechococcus*,

C1 has the lowest mixed-layer growth estimates, but that is the only cycle where growth consistently exceeds grazing and net growth is positive (Fig. 4G–I). Grazing notably exceeds growth at the offshore stations, giving the highest net negative growth rates for *Synechococcus* in the upper EZ for cycles C4 and C5. For picoeukaryotes, mean growth and grazing estimates for the upper 20 m are relatively similar (0.5–0.6 $\rm d^{-1}$) for the inshore cycles, giving slight net negative balances for C1–C3 (Fig. 4J-L). Grazing rates strongly exceed picoeukaryote growth rates for offshore cycle C5, with large net negative growth, as well as large measurement uncertainties, over most of the EZ.

3.4. Shipboard experiments

Shipboard incubations of the multi-treatment dilution experiments show similar Chla-based results for all cycles (Fig. 5). Regression slopes are linear and negative for all experiments, and nutrient-added growth rates (μ_n) fall in a similar range $(0.9–1.2~d^{-1})$ for inshore and offshore cycles. All experiments also show substantial differences between growth rates in the nutrient added and control bottles. The main differences among experiments are higher grazing mortality estimates for offshore $(0.41–0.47~d^{-1})$ than inshore $(0.24–0.29~d^{-1})$ cycles, higher net growth rates in control bottles for the offshore, and consequently higher μ_0 rates in the offshore $(0.75–0.76~versus~0.04-0.26~d^{-1})$.

Compared to Chla results, the rate estimates for picophytoplankton

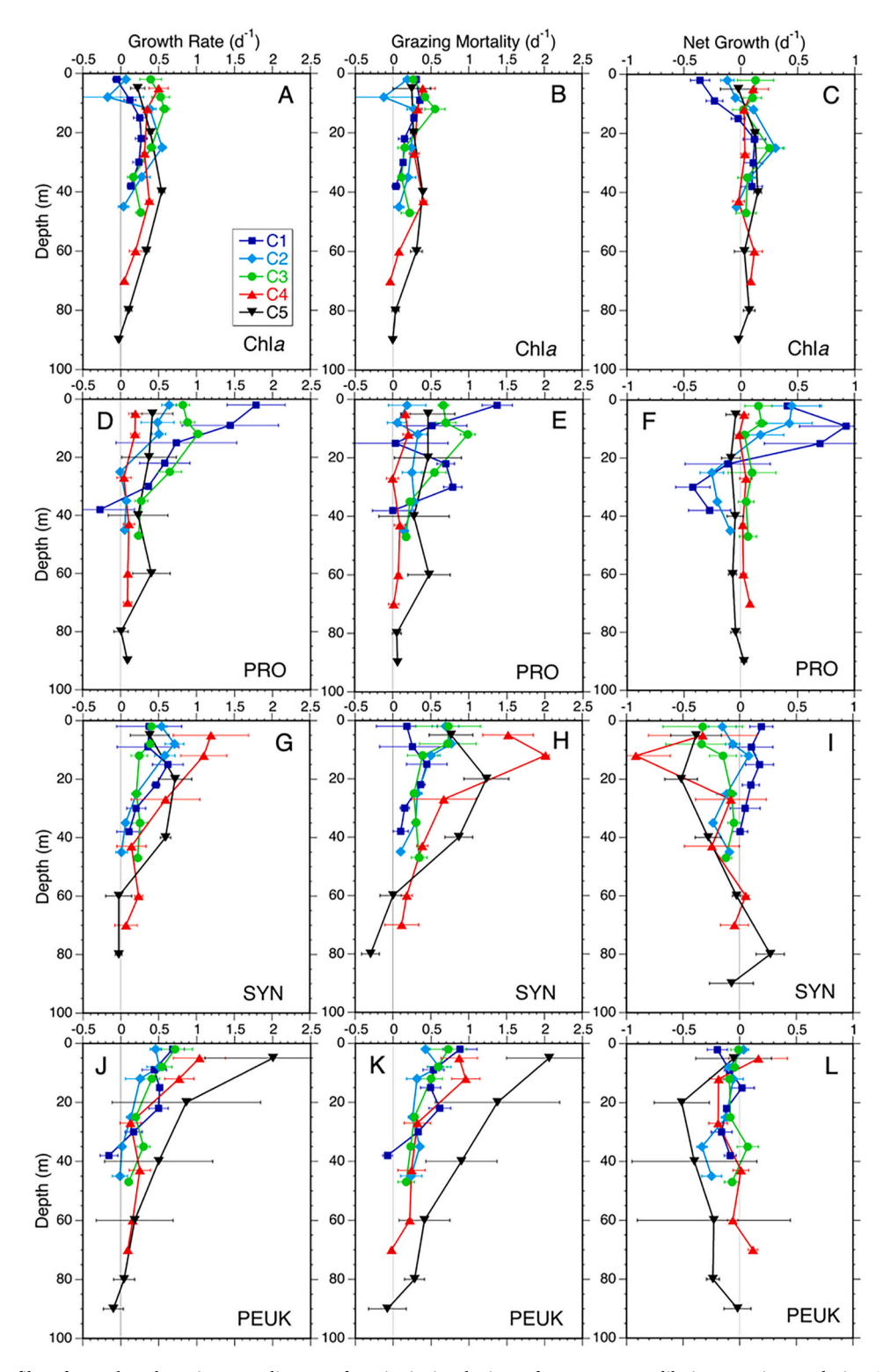


Fig. 4. Mean depth profiles of growth and grazing mortality rates from *in situ* incubations of two-treatment dilution experiments during Cycles 1–5. Chla = chlorophyll a; PRO = Prochlorococcus; SYN = Synechococcus; PEUK = picoeukaryotes. Net Growth (d^{-1}) is the difference between daily estimates of instantaneous Growth and Grazing Mortality. Uncertainties are standard errors of mean values.

populations from the same dilution experiments are more similar between offshore and inshore cycles and between growth rate determinations for nutrient-added and control bottles (Table 2). Averaging the rate estimates for all picophytoplankton populations, grazing mortalities are similar between offshore and inshore (0.47 \pm 0.13 versus 0.44 \pm 0.05 d $^{-1}$, respectively), and both are in the range of Chla estimates for the offshore, where picophytoplankton populations dominate.

Growth estimates from control bottles are comparable to μ_n rates for both <code>Synechococcus</code> (0.45 \pm 0.12 versus 0.49 \pm 0.06 d $^{-1}$) and picoeukaryotes (0.57 \pm 0.18 versus 0.60 \pm 0.05 d $^{-1}$). For <code>Prochlorococcus</code>, control growth rates are higher than nutrient added estimates on average (0.73 \pm 0.04 versus 0.49 \pm 0.07 d $^{-1}$) and for each experiment, suggesting a nutrient depression effect.

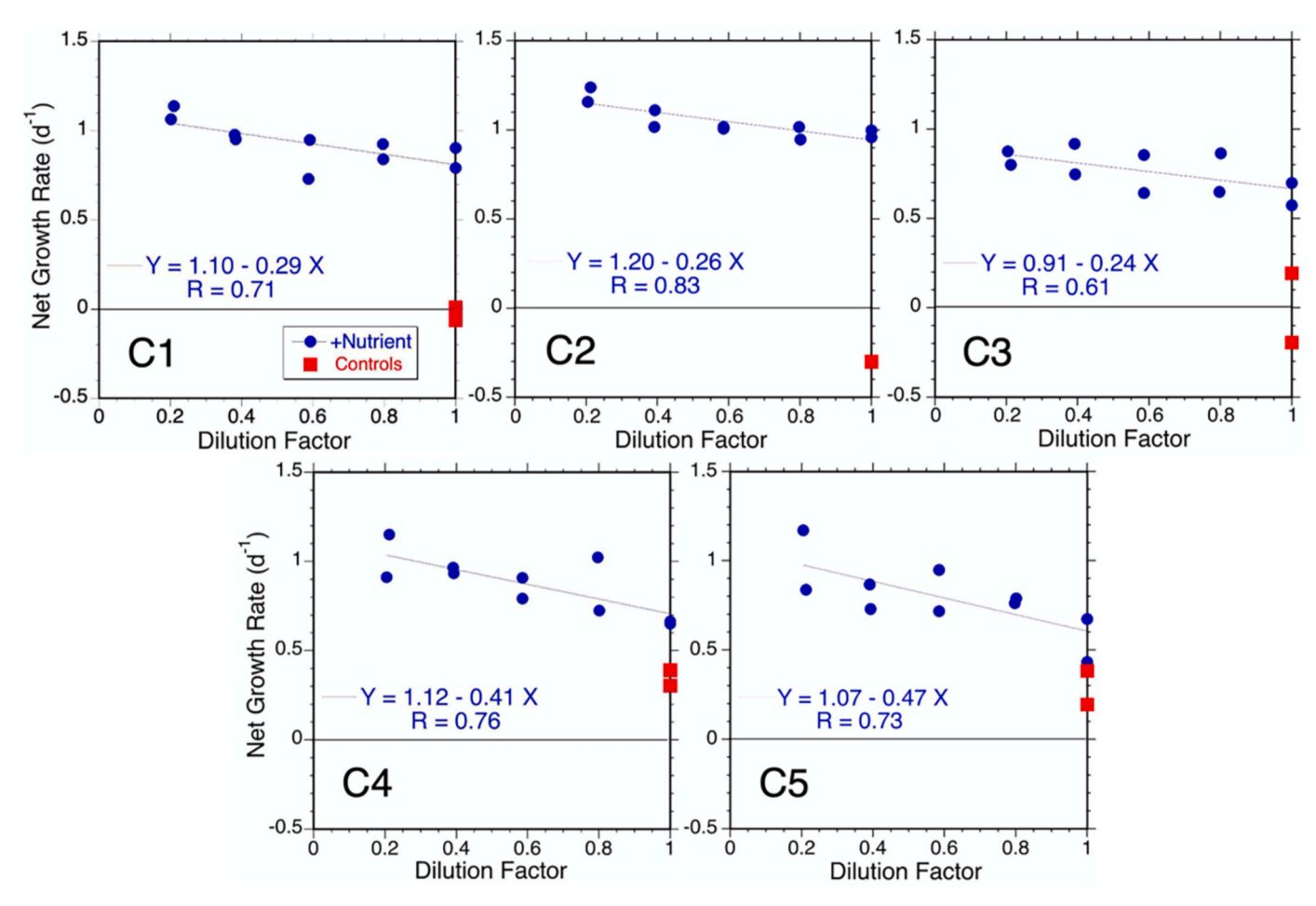


Fig. 5. Chlorophyll-based results from multi-treatment dilution experiments conducted during Cycles 1–5. Regressions are from nutrient-added dilution treatments. Controls demonstrate lower net growth rates without nutrient additions.

Table 2 Growth and grazing mortality rates for picophytoplankton populations from shipboard incubations of multi-treatment dilution experiments during Cycles 1–5. μ_n (d^{-1}) = growth rates in nutrient added incubations (regression intercept); m (d^{-1}) = grazing mortality rate (negative regression stope); μ_o (d^{-1}) = growth rates without added nutrients (net growth in seawater controls + m); R = correlation coefficient.

Cycle	Prochloro	ococcus (PRO)			Synechoc	Synechococcus (SYN)				Picoeukaryotes (PEUK)			
	μ_n	m	μ_{o}	R	μ_n	m	$\mu_{\rm o}$	R	μ_n	m	μ_{o}	R	
C1	0.63	0.35	0.90	0.55	1.04	0.46	0.98	0.88	1.30	0.72	0.75	0.94	
C2	0.35	0.57	0.68	0.90	0.51	0.51	0.47	0.95	0.57	0.44	0.61	0.84	
C3	0.55	0.43	0.59	0.93	0.30	0.33	0.27	0.92	0.37	0.18	0.28	0.55	
C4	0.63	0.40	0.79	0.88	0.42	0.06	-0.03	0.12	0.31	0.16	0.18	0.66	
C5	0.29	0.85	0.70	0.63	0.18	0.37	0.58	0.38	0.45	1.10	1.05	0.78	
ALL	0.49	0.52	0.73	0.78	0.49	0.35	0.45	0.65	0.60	0.52	0.57	0.75	

3.5. Net growth rate comparisons

Table 3 compares net growth rate estimates in the ambient water column to those from $in\ situ$ incubated bottles for each experimental cycle and for each stock measured. Both ambient and bottle rates vary from -0.3 to $0.3\ d^{-1}$ for individual cycles, but mean rates for all cycles are substantially more constrained. For example, stock-averaged net ambient rates vary narrowly from -0.03 to $0.01\ d^{-1}$ (Table 3), indicative of a general EZ balance between growth and grazing loss processes. Mean bottle estimates range from negative $(-0.11\ to\ -0.13\ d^{-1})$ for Synechococcus and picoeukaryotes to net positive $(0.07\ d^{-1})$ for Chla and Prochlorococcus. There is reasonable agreement between ambient and bottle rates for individual cycle experiments overall, but disparities arise mainly from large differences in one experiment for each population,

which is also a different cycle for each population. For *Prochlorococcus*, the main disparity is C2, where the large net decline in the ambient population is not predicted by bottle results (-0.25 versus $0.02~{\rm d}^{-1}$, respectively). For *Synechococcus*, the main disparity occurs in cycle C4 (0.16 versus $-0.21~{\rm d}^{-1}$). For picoeukaryotes, the largest disparity of all (0.5 ${\rm d}^{-1}$) occurs for cycle C5 (0.17 versus $-0.32~{\rm d}^{-1}$). Without these specific experiments, average net growth rates for ambient and bottle results in the remaining four cycles would be similar within 0.01 ${\rm d}^{-1}$ for *Prochlorococcus*, 0.02 ${\rm d}^{-1}$ for picoeukaryotes and 0.06 ${\rm d}^{-1}$ for *Synechococcus*.

3.6. Taxon composition from 18 S sequencing

Table 4 summarizes relative 18 S V9 sequence contributions for

Table 3

Net growth rates (d^{-1}) of phytoplankton chlorophyll a (Chla) and flow cytometry populations in the ambient water column and in experimental bottle incubations during P1408 Cycle 1–5 experiments in August 2014. PRO = Prochlorococcus; SYN = Synechococcus; PEUK = photosynthetic picoeukaryotes. Net Ambient rates are determined from changes in depth-integrated stocks measured in the water column on successive days following a satellite tracked drifter. Net Bottle rates are determined from depth-integrated, abundance-weighted rate measurements from experimental $in \, situ$ bottle incubations attached to the drift array. Uncertainties are standard errors of mean values for the three days of individual cycle experiments or 15 total days for ALL experiments combined.

Cycle	Chla	Chla	PRO	PRO	SYN	SYN	PEUK	PEUK
	Ambient	Bottle	Ambient	Bottle	Ambient	Bottle	Ambient	Bottle
C1	-0.10 ± 0.06	0.05 ± 0.08	0.21 ± 0.62	0.27 ± 0.27	0.26 ± 0.52	0.16 ± 0.07	-0.02 ± 0.14	-0.09 ± 0.03
C2	0.04 ± 0.09	0.09 ± 0.03	-0.25 ± 0.16	0.02 ± 0.12	-0.17 ± 0.07	-0.09 ± 0.01	-0.20 ± 0.09	-0.15 ± 0.05
C3	-0.02 ± 0.07	0.10 ± 0.05	-0.03 ± 0.27	0.10 ± 0.09	-0.11 ± 0.24	-0.16 ± 0.11	-0.11 ± 0.10	0.04 ± 0.03
C4	-0.02 ± 0.08	0.06 ± 0.03	0.08 ± 0.26	0.02 ± 0.03	0.16 ± 0.35	-0.21 ± 0.23	0.08 ± 0.12	-0.06 ± 0.06
C5	-0.04 ± 0.05	0.06 ± 0.01	-0.01 ± 0.27	-0.06 ± 0.06	-0.06 ± 0.29	-0.22 ± 0.04	0.17 ± 0.22	-0.32 ± 0.31
ALL	-0.03 ± 0.03	0.07 ± 0.02	0.00 ± 0.14	0.07 ± 0.06	0.01 ± 0.13	-0.11 ± 0.06	-0.02 ± 0.06	-0.13 ± 0.06

Table 4
Relative 18 S V9 sequence abundances of eukaryotic phytoplankton at inshore and offshore stations sampled on CCE Process cruises P1408, P0605 and P0704. C = experimental cycle number. Uncertainties are standard errors of mean values.

Taxon	P1408_C1	P1408_C2	P1408_C3	P1408_C4	P1408_C5	P0605_C1	P0704_C1
	Inshore	Inshore	Inshore	Offshore	Offshore	Inshore	Inshore
Dinophyceae_Gymnodiniales	28.1 ± 6.7	7.4 ± 1.9	21.9 ± 4.5	37.4 ± 2.0	36.6 ± 2.9	34.6 ± 9.0	13.1 ± 2.7
Dinophyceae_Gonyaulacales	8.5 ± 1.0	4.6 ± 1.0	0.6 ± 0.3	4.0 ± 2.7	0.5 ± 0.2	15.2 ± 4.5	1.9 ± 0.4
Dinophyceae_Peridiniales	5.6 ± 2.4	1.0 ± 0.0	1.9 ± 0.4	5.4 ± 0.5	6.5 ± 0.6	2.5 ± 1.0	16.0 ± 2.0
DinophyceaeDinophyceae_Other	26.5 ± 8.4	8.6 ± 1.5	18.5 ± 3.1	27.9 ± 3.7	29.3 ± 3.8	6.4 ± 0.7	8.9 ± 1.2
Chlorophyceae_Prasinophyceae	3.9 ± 2.0	48.7 ± 12	45.9 ± 10	10.6 ± 2.0	19.6 ± 5.6	0.0 ± 0.0	0.1 ± 0.0
Chlorophyceae_Ostreococcus	0.1 ± 0.0	0.2 ± 0.1	0.0 ± 0.0	0.0 ± 0.0	0.0 ± 0.0	0.1 ± 0.1	27.0 ± 9.7
Chlorophyceae_Micromonas	0.2 ± 0.1	0.8 ± 0.6	0.4 ± 0.2	0.0 ± 0.0	0.0 ± 0.0	0.1 ± 0.0	3.9 ± 0.5
Chlorophyceae_Bathycoccus	0.3 ± 0.1	0.9 ± 0.7	1.0 ± 0.4	0.6 ± 0.3	0.2 ± 0.1	0.0 ± 0.0	1.0 ± 0.2
Chlorophyceae_Other	0.2 ± 0.1	0.1 ± 0.1	0.1 ± 0.0	0.2 ± 0.1	0.1 ± 0.0	0.0 ± 0.0	0.2 ± 0.1
Stramenopile_Pennate Diatom	12.3 ± 4.2	11.5 ± 4.9	0.2 ± 0.1	3.2 ± 3.1	0.1 ± 0.0	6.1 ± 1.8	2.5 ± 0.4
Stramenopile_Polar Centric Diatom	2.6 ± 0.5	3.7 ± 2.4	0.1 ± 0.0	0.4 ± 0.4	0.0 ± 0.0	27.5 ± 7.9	10.2 ± 2.8
Stramenopile_Radial Centric Diatom	0.9 ± 0.2	2.3 ± 1.2	0.2 ± 0.1	0.1 ± 0.1	0.0 ± 0.0	6.0 ± 2.5	2.4 ± 0.7
Stramenopile_MAST3	7.2 ± 1.9	3.8 ± 1.7	0.3 ± 0.1	1.0 ± 0.2	0.8 ± 0.1	0.1 ± 0.0	0.2 ± 0.1
Stramenopile_Pelagophyceae	0.3 ± 0.1	0.8 ± 0.5	2.8 ± 0.9	0.8 ± 0.6	0.2 ± 0.0	0.0 ± 0.0	0.1 ± 0.1
Stramenopile_Other	1.9 ± 0.9	3.2 ± 1.4	1.8 ± 0.6	3.2 ± 0.6	2.4 ± 0.4	0.4 ± 0.2	1.8 ± 0.6
Hacrobia_Prymnesiophyceae	0.4 ± 0.1	1.1 ± 0.6	2.3 ± 0.7	3.5 ± 0.3	2.5 ± 0.3	0.3 ± 0.1	6.8 ± 1.5
Hacrobia_Cryptophyceae	0.1 ± 0.0	0.2 ± 0.1	0.1 ± 0.0	0.2 ± 0.0	0.1 ± 0.0	0.1 ± 0.0	3.1 ± 0.4

inshore and offshore stations sampled during the warm-anomaly summer cruise (P1408) in comparison to samples taken previously from springtime coastal blooms (P0605, P0704). Since the aim was to correspond as closely as possible to free-living eukaryotic phytoplankton, relative sequence contributions are based on the total sequences remaining after removing reads for prokaryotes, metazoans, ciliates, rhizaria and the mainly parasitic dinoflagellates (Syndiniales).

Samples from the P1408 summer cruise are notably distinguished by large sequence contributions of Prasino Clade 7. Prasino Clade 7B1 cells dominate at inshore stations, and Clade 7A1 cells dominate in offshore samples with Clade 7B2 of significant but secondary importance. Sequence reads for pennate diatoms (11.3–12.5%) and MAST3 Stramenopiles (3.8–7.2%) are also more represented in C1 and C2 P1408 inshore samples than in others. The latter are mainly *Solenicola* sp., and *Pseudonitzschia fradulenta* is the dominant pennate. In comparison, *Pseudonitzschia australis* and *P. hemi* were more important in P0605 and P0704 upwelling samples. The large sequence contribution of *Ostreococcus* sp. in P0704 samples (27%) is almost entirely Clade A, which is also the main type, though less abundant, in samples from P1408 and P0605.

Among dinoflagellate taxa, the Gymnodiniales are substantial contributors to sequence reads (7–37%) and consistently dominated by *Karlodinium micrum* in all samples (Table 4). Gonyaulacales sequences are also similarly dominated by one taxon, *Neoceratium tenue*, at all sites, but conspecific *N. fusus* makes a large secondary contribution to the P0605 bloom. *Heterocapsa rotundata* is the major Peridinales taxon and the most important contributor over all dinoflagellate groups in the P0704 bloom samples, while *Luciella* sp. and *Blastodinium oviforme*

contribute most to sequence abundances in P1408 offshore and P0605 samples, respectively. Sequences in the Other Dinoflagellate category are mainly uncultivated forms.

For radially centric diatoms, sequences for the spring upwelling blooms (P0605, P0704) are dominated by *Rhizosolenia setigera*, while *Proboscia alata* contributes most at P1408 inshore stations. For polar centrics, *Thalassiosira* sp. notably dominates in the P0605 and P0704 bloom samples where the total polar centric contribution is highest (10–28%). *Eucampia zoodiacus* and *Thalassiosira* sp. are the main contributors at P1408 inshore stations C1 and C2. The P0605 bloom also had substantial sequence contributions from *Skeletonema* and *Coscinodiscus* spp., which were generally rare in other samples.

Results from the 18 S V4 sequence analyses were not as complete as the V9 analyses (missing C1 samples and poor read 2 quality) and differed in some respects. We highlight these difference in Fig. 6, which considers relative sequence contributions of taxonomic groups that are known to be small free-living cells, hence most likely the cells comprising the category of picoeukaryotes in P1408 experiments. As in the V9 reads, Prasino clades stand out as the notably dominant group in the P1408 eukaryote community, accounting for 54-73% of sequences attributed to picoeukaryotes in C3-C5. One major difference is the large percentage of prymnesiophyte reads (22-55%) in the V4 sequences, which do not appear for V9 (Table 4). Cycle 2 is also unusual in the V4 sequence reads with Ostreococcus comprising a relatively high percentage (18%) of reads and Prasino clades a much reduced percentage (12%), whereas C2 and C3 show similar Ostreococcus in V9 sequence results, with Prasino clades highly dominant and Ostreococcus poorly represented (Fig. 6, Table 4).

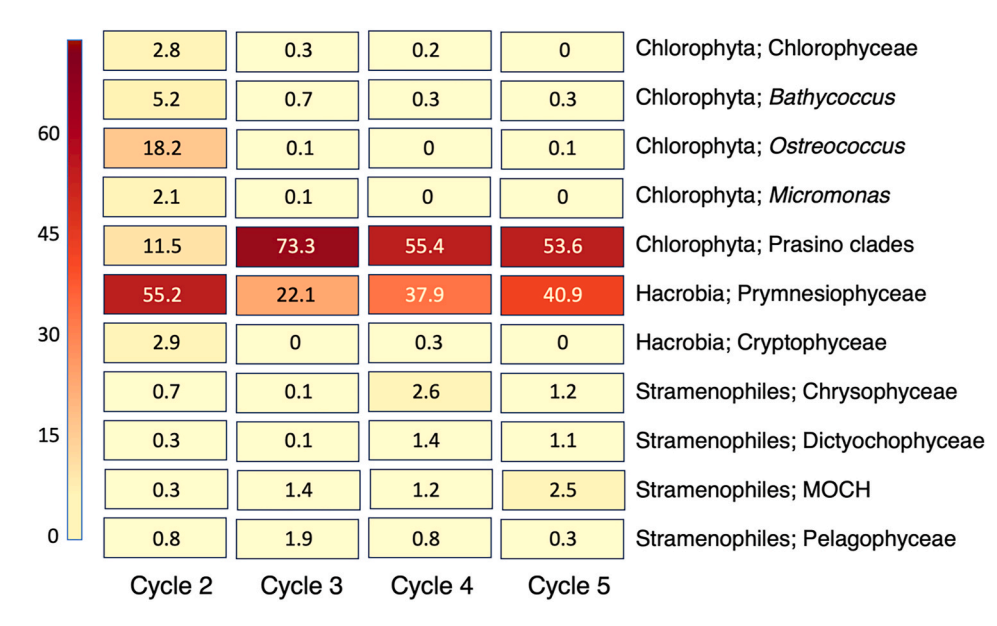


Fig. 6. Percent sequence abundances from 18 S V4 analyses for known picoeukaryote taxa in seawater samples collected in the upper euphotic zone during P1408 cycles C2–C5.

4. Discussion

4.1. Physical circulation and environmental conditions during P1408

Physical circulation in the Point Conception study region during August 2014 can be reasonably inferred from the drifter trajectories and satellite Chla imagery shown in Fig. 1. Onshore flow of surface waters moved a tongue of low Chla shoreward during experiments C4 and C3, compressing a thin region of elevated Chla along the coast and forcing northwestward transport north of the Point in C1 and southwestward transport south of the Point in C2. Consistent with this interpretation, environmental conditions and populations for C1 appear representative of waters originating closest to the coast, and C3 combines strong offshore influences on Chla and Prochlorococcus abundance with mixed offshore-onshore characteristics in temperature, salinity, Synechococcus and picoeukaryotes. Surface water transport was not clearly related to local wind stress measured continuously by the ship's MET system, which remained upwelling favorable but relatively weak with a mean V component of -10.7 km h^{-1} (range $-0.4 \text{ to } -28.5 \text{ km h}^{-1}$) from 5 days before C1 through the end of C5. Nitrate profiles do, however, show evidence of weak upwelling, with the nitracline lifted into the lower euphotic zone of inshore stations, but not breaking into the surface mixed layer (Fig. 2).

Based on data from nine fixed stations sampled quarterly on CalCOFI cruises from 2004 through 2015, the 2014–15 warm anomaly averaged $+2\,^{\circ}\mathrm{C}$ above seasonal mixed-layer values and extended relatively uniformly from 35 to 700 km seaward (Fig. 1, Landry et al., 2024). Within this broad area, summer-fall mixed layer nitrate concentrations were 10-fold lower in 2014–15 than baseline years at inshore stations (within 200 km of the coast) and 6-fold lower in offshore waters. Mean nitracline depths were also 16 and 24 m deeper than normal for inshore and offshore locations, respectively, and density stratification between the nitracline and mixed layer was stronger in 2014–15 than during baseline years.

Because the P1408 cruise occupied just one month of the much longer warm anomaly event (Fig. 1), its conditions are not necessarily representative of the 2014–15 averages. Comparisons of C1–C5 mean values to warm-anomaly values with distance from shore do indicate that offshore conditions of temperature, surface nitrate concentration, nitracline depth and density stratification during P1408 conformed closely to 2-year summer-fall anomaly conditions (Landry et al., 2024).

However, conditions for the inshore cycles (C1–C3) for P1408 were less extreme than 2014-15 summer-fall averages, with mixed-layer temperature and stratification strength closer to the 2004-13 baseline trends with distance from shore and nitrate concentration and nitracline depth intermediate between baseline and warm-anomaly trends. These observations suggest that P1408 captured an early phase of the 2014-15 MHW off of southern California, when stronger conditions of stratification and nutrient decline were still building, coincident with warmer-stratified offshore waters advancing shoreward and suppressing upwelling, as indicated by the drifter trajectories in Fig. 1.

4.2. Picophytoplankton abundances and community composition

Increasing importance of picophytoplankton cells is one of the predicted outcomes of a warmer strongly-stratified ocean with reduced nutrient fluxes to surface waters (Bopp et al., 2013; Flombaum et al., 2020). P-line surveys in the Gulf of Alaska suggested such a shift to smaller cells during the 2014-15 MHW based on higher concentrations of cyanobacteria-associated pigments (Peña et al., 2019; Wyatt et al., 2022). In the SCCS, combined flow cytometric and microscopical analyses confirm that the picophytoplankton contributed significantly more to total phytoplankton C in 2014–15 (44.0 \pm 2.3%) than in 2004–13 baseline years (37.7 \pm 1.4%) (Landry et al., 2024), but details and directions varied among populations. Prochlorococcus was solely responsible for the overall increase in picophytoplankton C, with higher inshore and offshore abundances during 2014-15 but larger relative change inshore (Landry et al., 2024). In contrast, Synechococcus and picoeukaryotes generally declined during 2014-15, with greater relative change in the offshore.

Both directions of these warm-anomaly responses can be understood as shifts in the typical picophytoplankton distributional patterns for the region, which have population biomass maxima at intermediate values of Chla and primary production and declining abundances in richer coastal waters (Taylor and Landry, 2018; Landry et al., 2023). Prochlorococcus abundances are typically high in offshore oligotrophic waters and decline sharply with increasing system richness. A shoreward shift of this distributional pattern increases Prochlorococcus abundances everywhere, but especially in coastal waters where cell abundances are generally very low and often zero. Synechococcus and picoeukaryotes have biomass maxima at higher values of Chla and closer to shore than Prochlorococcus and decline more sharply in nutrient-poor offshore

waters (Taylor and Landry, 2018). A strong shoreward shift of this pattern decreases *Synechococcus* and picoeukaryote abundances generally across the region, but especially in the offshore. A simple shoreward-shift interpretation is also supported by transport inferences above from the drifter trajectories, but leaves open the possibility that more subtle effects, like selection for different ecotypes of photosynthetic bacteria (Larkin et al., 2020), also occurred as the populations adapted to warmer, nutrient-poor conditions.

For eukaryotic phytoplankton, 18 S sequence analyses allow taxonomic comparisons of community composition among P1408 experimental cycles and two prior coastal upwelling events but leave many important questions open. For example, while the notably high relative abundances of Chlorophyceae, especially Prasino clades, both inshore and offshore during P1408 (Table 4; Fig. 6) could well be a characteristic of MHWs, the current data are too temporally and spatially sparce to support such a conclusion. The next available 18 S data with the same V9 primers show greatly reduced Chlorophyceae represented mainly by Ostreococcus and Micromonas at the end of the warm anomaly in April 2016 (P1604) (Valencia et al., 2021, 2022), but they are also from a different season (spring versus summer). Although V9 sequences suggest otherwise, plasmid reads and microscopical analyses support V4 results (Fig. 6) about the presence of significant prymensiophytes during P1408 (Freibott, 2017). According to the latter, prymesiophytes accounted for up to 55% and averaged 15.1 \pm 2.5% of the C biomass of <5- μm eukaryotes during the 2014-15 heat wave. However, 2004-13 baseline values were almost 3 times higher (40.7 \pm 1.9%). Thus, prymesiophytes were likely secondary to prasinophytes as contributors to picoeukaryotes during the warm anomaly but appear to be substantially more important in the small size fraction during normal conditions.

Although offshore experiments C4 and C5 are separated by substantial distances (Fig. 1), their similar community compositions are consistent with having experienced similar environmental forcing in oligotrophic waters. In contrast, high compositional variability is a notable feature of the inshore region, presumably reflecting environmental selection for different forms that arise seasonally or interannually at a given location as well as some apparent randomness in community assembly at sites in close proximity. The former are illustrated by the dominance of pennate diatoms during P1408 suppressedupwelling conditions as opposed to centric diatoms during normal (P0605-P0704) upwelling blooms and by large differences in dinoflagellate and chlorophyte group contributions between P0605 and P0704 blooms (Table 4). The latter are illustrated by the substantial differences in prasinophyte and dinoflagellate group contributions in waters with close spatial origins for C1 and C2 experiments. For experiments separated by only a few days, it is also clear that advective transport was bringing another arrangement of taxa (C3) with mixed offshore and inshore affinities into the same area.

4.3. Nutrient effects

In full dilution experiments, growth rate differences between nutrient-added (μ_n) and no-nutrient control (μ_o) bottles can be taken as an indication of possible nutrient limitation effects (Landry et al., 1998). For Synechococcus and picoeukaryotes, μ_n and μ_o estimates were similar in many individual experiments and showed no systematic differences on average (0.49 versus 0.45 d $^{-1}$ for Synechococcus; 0.60 versus 0.57 d $^{-1}$ for picoeukaryotes; Table 2). For Prochlorococcus, μ_o estimates exceeded μ_n in all experiments (mean values of 0.73 versus 0.49 d $^{-1}$, respectively), suggesting a growth rate suppression with added nutrients. The lack of an observable stimulatory effect of added nutrients indicates that cell division rates of small phototrophs represented those for ambient nutrient concentrations during our 24-h incubations.

The contrasting large differences in Chla net growth rates with and without nutrients (Fig. 5) can likely be attributed to a general physiological shift up in cell Chla content in the nutrient-added treatments. We note, for example, that even though *Synechococcus* and picoeukaryotes

did not show a cell division response to added nutrients in the dilution incubations, they did each show strong nutrient-added up-shifts in cellular red-fluorescence (a Chla indicator) in the FCM-analyzed populations that corresponded to cellular Chla increases of 0.3-0.6 d⁻¹ at inshore stations where Synechococcus and picoeukaryotes were most abundant. In contrast, Prochlorococcus showed insignificant change $(0.02 \pm 0.06 \,\mathrm{d}^{-1})$ in cell Chla content in no-nutrient and nutrient-added treatments over all experiments. We interpret these differences as Synechococcus and picoeukaryotes being physiogically limited by ambient nutrient availability, while Prochlorococus was not. We also consider that the same phenomenon – Chla response to added nutrients precedes change in cell division rate by more than the one day of our dilution incubations - applies to our two-treatment dilution results for Chla without nutrients, which should therefore represent cell-specific rates at ambient nutrient concentrations. That we find smaller Chla net-growth differences between nutrient added and control bottles in offshore (C4–C5) experiments is consistent with *Prochlorococcus* (not responsive to nutrients) being the biomass dominant in those waters, while the much larger differences for inshore (C1-C3) experiments involve cell Chla responses of *Synechococcus*, picoeukaryotes and larger taxa.

4.4. Heat wave impacts on phytoplankton dynamics and food web interactions

By design, CCE Process cruises exploit large spatial gradients in food web structure and rates between SCCS onshore and offshore waters as analogs for understanding how the pelagic community might respond to future change in environmental conditions (Ohman et al., 2013). Consistent with the underlying assumptions of this space-for-time approach, the functional relationships for mesozooplankton grazing and egg (secondary) production relative phytoplankton (Chla) biomass were similar during MHW cruises and normal environmental conditions, and carbon export, another process tied to mesozooplankton activity, also indicated no substantial differences relative to primary production and mesozooplankton grazing compared to previous cruises (Morrow et al., 2018; Nickels and Ohman, 2018). Here we consider how lower food web dynamics during August 2014 align with these findings.

For eight CCE Process cruises compared on the same basis (upper 4 experimental depths, similar primary production of 10-100 mg C m⁻³ $d^{-1}),\,P1408$ inshore rate estimates for Prochlorococcus ($\mu=0.78~d^{-1},\,m$ $= 0.54 \ d^{-1}$) are higher than average ($\mu = 0.48 \ d^{-1}$, $m = 0.34 \ d^{-1}$; Landry et al., 2023) and show higher-than-average net positive growth. For Synechococcus and picoeukaryotes, P1408 growth rates are similar to average $(0.41-0.43 \text{ d}^{-1} \text{ versus } 0.38-0.44 \text{ d}^{-1}, \text{ respectively})$, but grazing mortality rates are substantially higher than average (0.47-0.51 d versus 0.30–0.34 d⁻¹). While our short-term experimental results cannot be extrapolated to the full MHW duration, rate trends during this early phase are at least consistent with observations that Prochlorococcus increased at inshore locations during 2014-15 while Synechococcus and picoeukaryotes generally declined (Landry et al., 2024). In our experiments, these trends are associated with increasing growth rate relative to grazing loss for Prochlorococcus but are mainly driven by increased grazing mortality of Synechococcus and picoeukaryotes.

At the community level, trophic processes during the suppressed upwelling conditions of August 2014 are characterized by an increased grazing role of microzooplankton at inshore stations, which comes at the expense of direct grazing impact of mesozooplankton. In previous experiments conducted during active SCCS upwelling, mesozooplankton grazing consumed up to 150% of daily phytoplankton production (PP) and was the main determinant of whether phytoplankton biomass increased (P0605) or decreased (P0704) (Landry et al., 2009). Microzooplankton grazing during these active upwelling conditions, averaging 50% of PP, was not trival but substantially below the global average of \sim 67% (Calbet and Landry, 2004; Steinberg and Landry, 2017). At comparable inshore locations (C1–C3) during P1408, microzooplankton grazing averaged 80.5 \pm 4.4% of PP, identical to

microzooplankton grazing impact (80.4 \pm 2.9%) for offshore cycles C4 and C5. Similarly low net growth rate of the ambient phytoplankton community (Chla) at both inshore and offshore locations (Table 3) is another indication of comparable balanced dynamics during August 2014

Morrow et al. (2018) reported slightly lower mass-specific rates of mesozooplankton grazing based on Chla ingested during warm-anomaly compared to normal conditions, but those results were not statistically significant and do not consider compensatory changes in dietary composition. Based on phytoplankton carbon biomass estimates from microscopical analyses, for example, C:Chla ratios for inshore locations during the 2014-15 MHW are about two-fold richer in C than those for the P0605-P0704 upwelling experiments used for grazing rate comparisons (85 \pm 8 versus 41 \pm 2, respectively; Landry et al., 2024). Additionally, C and N intake by mesozooplankton would be augmented by the shift to increased trophic flow through the microzooplankton grazing pathway (Stukel et al., 2011; Landry and Décima, 2017). Assuming a 30% gross growth efficiency for microzooplankton production and steady-state flow to mesozooplankton consumers (Landry and Calbet, 2004), a shift in microzooplankton grazing from 50 to 80% of PP would be equivalent to mesozooplankton directly consuming an extra 9% of PP without a marker that registers as Chla ingestion. Compared to Chla-based mesozooplankton grazing measurements during normal upwelling conditions, the combined effects of greater dietary contribution from microzooplankton and richer C:Chla content from phytoplankton at inshore stations during the warm anomaly might reasonably account for a factor of three difference in C ingested relative to Chla consumed.

5. Conclusions

Experimental studies in August 2014 captured the normally dynamic region off Point Conception during the early phase of the 2014-15 MHW, before onshore waters had fully achieved the mean anomalous conditions of temperature, stratification strength and nutrient depletion for the two-year period. Physical circulation during August 2014 was consistent with transport of warm-stratified offshore waters shoreward, suppressing upwelling and shifting picophytoplankton distributions to increased onshore abundance of Prochlorococcus and decreased abundances of Synechococcus and picoeukaryotes, both observed MHW effects. These trends were reinforced by higher-than-average net growth (growth-grazing difference) of Prochlorococcus at inshore sites and grazer-driven population declines of Synechococcus and picoeukaryotes relative to previous experimental results at comparable primary production. Despite substantial spatial variability in phytoplankton composition, community dynamics at offshore and inshore experimental locations were both close to steady state and with microzooplankton consuming similar percentages (80%) of primary production. We thus confirm expectations that the 2014-15 MHW resulted in greater trophic flow through the microbial food web, at the expense of reduced phytoplankton (Chla) consumption by mesozooplankton. However, compensatory changes in phytoplankton C:Chla and increased predation on protistan microzooplankton can partially offset the decline in direct herbivory and need to be considered in assessing the full MHW impact on mesozooplankton energetics.

CRediT authorship contribution statement

Michael R. Landry: Writing – original draft, Supervision, Project administration, Methodology, Investigation, Formal analysis, Data curation, Conceptualization. Alexandra L. Freibott: Writing – review & editing, Methodology, Investigation, Formal analysis. Michael R. Stukel: Writing – review & editing, Investigation. Karen E. Selph: Writing – review & editing, Methodology. Andrew E. Allen: Writing – review & editing, Methodology. Ariel Rabines: Writing – review & editing, Methodology.

Declaration of competing interest

The authors declare that they have no known competing financial interests or personal relationships that could have appeared to influence the work reported in this paper.

Data availability

Data will be made available on request.

Acknowledgements

This study was supported by U.S. National Science Foundation grants OCE-0417616, OCE-1026607 and OCE-1637632 to the CCE LTER Program and by a Scripps Institution of Oceanography Mullin Fellowship to A.L.F. for molecular sample analyses. We thank captains and crews of R/Vs *Melville*, *Knorr* and *Thompson* as well as numerous cruise participants for their many contributions to the success of CCE Process cruises.

References

- Bond, N.A., Cronin, M.F., Freeland, H., Mantua, N., 2015. Causes and impacts of the 2014 warm anomaly in the NE Pacific. Geophys. Res. Lett. 42 https://doi.org/
- Bopp, L., et al., 2013. Multiple stressors of ocean ecosystems in the 21st century: projections with CMIP5 models. Biogeosci 10, 6225–6245. https://doi.org/10.5194/bg-10-6225-2013.
- Calbet, A., Landry, M.R., 2004. Phytoplankton growth, microzooplankton grazing and carbon cycling in marine systems. Limnol. Oceanogr. 49, 51–57. https://doi.org/ 10.4319/lo.2004.49.1.0051.
- de Vargas, C., et al., 2015. Eukaryotic plankton diversity in the sunlit ocean. Science 348 (6237), 1261605. https://doi.org/10.1126/science.1261605.
- Di Lorenzo, E., Mantua, N., 2016. Multi-year persistence of the 2014/15 North Pacific marine heatwave. Nat. Clim. Change 6, 1042–1047. https://doi.org/10.1038/ nclimate3082.
- Edgar, R.C., 2010. Search and clustering orders of magnitude faster than BLAST. Bioinformatics 26, 2460–2461. https://doi.org/10.1093/bioinformatics/btq461.
- Flombaum, P., Wang, W.L., Primeau, F.W., Martiny, A.C., 2020. Global picophytoplankton niche partitioning predicts overall positive response to ocean warming. Nat. Geosci. 13, 116–120. https://doi.org/10.1038/s41561-019-0524-2.
- Freibott, A.L., 2017. Plankton Community Composition and Grazing Dynamics in Upwelling Regions of the Pacific Ocean. Scripps Institution of Oceanography, University of California, San Diego, p. 160. Ph.D. Dissertation. https://escholarship.org/uc/item3993b1q1.
- Frölicher, T.L., Laufkötter, C., 2018. Emerging risks from marine heat waves. Nat. Comm. 9, 650. https://doi.org/10.1038/s41467-018-03163-6.
- Gómez-Ocampo, E., Gaxiola-Castro, G., Durazo, R., Beier, E., 2017. Effects of the 2013-16 warm anomalies on the California Current phytoplankton. Deep-Sea Res. II 151, 64–76. https://doi.org/10.1016/j.dsr2.2017.01.005.
- Kahru, M., Jacox, M.G., Ohman, M.D., 2018. CCE1: decrease in the frequency of oceanic fronts and surface chlorophyll concentration in the California Current System during the 2014–2016 northeast Pacific warm anomalies. Deep-Sea Res. I 140, 4–13. https://doi.org/10.1016/j.dsr.2018.04.007.
- Kintish, E., 2015. 'The Blob' invades Pacific, flummoxing climate experts. Science 348, 17–18. https://doi.org/10.1126/science.348.6230.17.
- Landry, M.R., Brown, S.L., Campbell, L., Constantinou, J., Liu, H., 1998. Spatial patterns in phytoplankton growth and microzooplankton grazing in the Arabian Sea during monsoon forcing. Deep-Sea Res. II 45, 2353–2368. https://doi.org/10.1016/S0967-0645(98)00074-5.
- Landry, M.R., Brown, S.L., Rii, Y.M., Selph, K.E., Bidigare, R.R., Yang, E.J., Simmons, M. P., 2008. Depth-stratified phytoplankton dynamics in Cyclone *Opal*, a subtropical mesoscale eddy. Deep-Sea Res. II 55, 1348–1359. https://doi.org/10.1016/j.dsr2.2008.02.001
- Landry, M.R., Calbet, A., 2004. Microzooplankton production in the oceans. ICES J. Mar. Sci. 61, 501–507. https://doi.org/10.1016/j.icesims.2004.03.011.
- Landry, M.R., Décima, M.R., 2017. Protistan microzooplankton and the trophic position of tuna: Quantifying the trophic link between micro- and mesozooplankton in marine food webs. ICES J. Mar. Sci. 74, 1885–1892. https://doi.org/10.1093/ icesims/fsx006.
- Landry, M.R., Freibott, A.L., Beatty, J.L.A., Selph, K.E., 2024. Phytoplankton biomass responses to a marine heat wave align with altered nitracline depth. Limnol. Oceanogr. 69 https://doi.org/10.1002/lno.12624.
- Landry, M.R., Haas, L.W., Fagerness, V.L., 1984. Dynamics of microplankton communities: experiments in Kaneohe Bay, Hawaii. Mar. Ecol. Prog. Ser 16, 127–133. https://doi.org/10.3354/meps016127.
- Landry, M.R., Hassett, R.P., 1982. Estimating the grazing impact of marine micro-zooplankton. Mar. Biol. 67, 283–288. https://doi.org/10.1007/BF00397668.
- Landry, M.R., Ohman, M.D., Georicke, R., Stukel, M.R., Tsyrklevich, K., 2009.

 Lagrangian studies of phytoplankton growth and grazing relationships in a coastal

- upwelling ecosystem off Southern California. Prog. Oceanogr. 83, 208–216. https://doi.org/10.1016/j.pocean.2009.07.026.
- Landry, M.R., Selph, K.E., Taylor, A.G., Décima, M., Balch, W.M., Bidigare, R.R., 2011.
 Phytoplankton growth, grazing and production balances in the HNLC equatorial
 Pacific. Deep-Sea Res. II 58, 524–535. https://doi.org/10.1016/j.dsr2.2010.08.011.
- Landry, M.R., Stukel, M.R., Selph, K.E., Goericke, R., 2023. Coexisting picoplankton experience different relative grazing pressures across an ocean productivity gradient. Proc. Natl. Acad. Sci. U.S.A. 120 (44), 1–8. https://doi.org/10.1073/ pnas.2220771120, 2220771120.
- Larkin, A.A., Moreno, A.R., Fagan, A.J., Fowlds, A., Ruiz, A., Martiny, A.C., 2020.
 Persistent El Niño driven shifts in marine cyanobacteria populations. PLoS One 15, e0238405. https://doi.org/10.1371/journal.pone.0238405.
- Leising, A.W., et al., 2015. State of the California current 2014-15: impacts of the warmwater "blob". CALCOFI (Calif. Coop. Ocean. Fish. Investig.) Rep. 56, 31–68. https://ir.library.oregonstate.edu/concern/articles/h989r499g.
- Lessard, E.J., Murrell, M.C., 1998. Microzooplankton herbivory and phytoplankton growth in the northwestern Sargasso Sea. Aquat. Microb. Ecol. 16, 173–188. https:// doi.org/10.3354/ame016173.
- Mahé, F., Rognes, T., Quince, C., de Vargas, C., Dunthorn, M., 2014. Swarm: robust and fast clustering method for amplicon-based studies. PeerJ 2. https://doi.org/ 10.7717/peerj.593.
- McCabe, R.M., et al., 2016. An unprecedented coastwide toxic algal bloom linked to anomalous ocean conditions. Geophys. Res. Lett. 43 (10) https://doi.org/10.1002/ 2016GL070023, 366-10.376.
- McClatchie, S., et al., 2016. State of the California current 2015-16: comparisons with the 1997-98 El Niño. CALCOFI (Calif. Coop. Ocean. Fish. Investig.) Rep. 57, 1–57. htt ps://escholarship.org/uc/item/730558jh.
- Monger, B.C., Landry, M.R., 1993. Flow cytometric analysis of marine bacteria with Hoechst 33342. Appl. Environ. Microbiol. 59, 905–911. https://doi.org/10.1128/ aem.59.3.905-911.1993.
- Morrow, R.M., Ohman, M.D., Goericke, R., Kelly, T.B., Stephens, B.M., Stukel, M.R., 2018. Cce V: primary production, mesozooplankton grazing, and the biological pump in the California Current Ecosystem: variability and response to El Niño. Deep-Sea Res. I 140, 52–62. https://doi.org/10.1016/j.dsr.2018.07.012.
- Nickels, C.F., Ohman, M.D., 2018. CCEIII: persistent functional relationships between copepod egg production rates and food concentration through anomalously warm conditions in the California Current Ecosystem. Deep-Sea Res. I 140, 26–35. https:// doi.org/10.1016/j.dsr.2018.07.001.
- Peña, M.A., Nemcek, N., Robert, M., 2019. Phytoplankton responses to the 2014–2016 warming anomaly in the northeast subarctic Pacific Ocean. Limnol. Oceanogr. 64, 515–525. https://doi.org/10.1002/lno.11056.

- Peterson, W., Robert, M., Bond, N., 2015. The warm blob conditions in the northeastern Pacific Ocean. PICES Press 23, 37–38.
- Selph, K.E., Landry, M.R., Taylor, A.G., Gutiérrez-Rodríguez, A., Stukel, M.R., Wokuluk, J., Pasulka, A.L., 2016. Phytoplankton production and taxon-specific growth rates in the Costa Rica Dome. J. Plankton Res. 38, 199–215.
- Selph, K.E., Landry, M.R., Taylor, A.G., Yang, E.-J., Measures, C.I., Yang, J.J., Stukel, M. R., Christensen, S., Bidigare, R.R., 2011. Spatially-resolved taxon-specific phytoplankton production and grazing dynamics in relation to iron distributions in the Equatorial Pacific between 110 and 140°W. Deep-Sea Res. II 58, 358–377. https://doi.org/10.1016/j.dsr2.2010.08.014.
- Shanks, A.L., et al., 2020. Marine heat waves, climate change, and failed spawning by coastal invertebrates. Limnol. Oceanogr. 65, 627–636. https://doi.org/10.1002/lno.1133
- Steinberg, D.K., Landry, M.R., 2017. Zooplankton and the ocean carbon cycle. Ann. Rev. Mar. Sci 9, 413–444. https://doi.org/10.1146/annurev-marine-010814-015924.
- Stukel, M.R., Landry, M.R., Benitez-Nelson, C.R., Goericke, R., 2011. Trophic cycling and carbon export relationships in the California Current Ecosystem. Limnol. Oceanogr. 56, 1866–1878. https://doi.org/10.4319/lo.2011.56.5.1866.
- Taylor, A.G., Landry, M.R., 2018. Phytoplankton biomass and size structure across trophic gradients in the southern California Current and adjacent ocean ecosystems. Mar. Ecol Prog. Ser. 592, 1–17. https://doi.org/10.3354/meps12526.
- Valencia, B., Stukel, M.R., Allen, A.E., McCrow, J.P., Rabines, A., Palenik, B., Landry, M. R., 2021. Relating sinking and suspended microbial communities in the California Current Ecosystem: digestion resistance and the contributions of phytoplankton taxa to export. Environ. Microbiol. 23, 6734–6748.
- Valencia, B., Stukel, M.R., Allen, A.E., McCrow, J.P., Rabines, A., Landry, M.R., 2022. Microbial communities associated with sinking particles across an environmental gradient from coastal upwelling to the oligotrophic ocean. Deep-Sea Res. I 179, 103668. https://doi.org/10.1016/j.dsr.2021.103668.
- Wyatt, A.M., Resplandy, L., Marchetti, A., 2022. Ecosystem impacts of marine heat waves in the northeast Pacific. Biogeosci 19, 5689–5705. https://doi.org/10.5194/bg-19-5689-2022.
- Xu, T., Newman, M., Capotondi, A., Di Lorenzo, E., 2021. The continuum of northeast Pacific marine heatwaves and their relationship to the tropical Pacific. Geophys. Res. Lett. 48, 2020GL090661 https://doi.org/10.1029/2020GL090661.
- Zaba, K.D., Rudnick, D.L., 2016. The 2014-2015 warming anomaly in the Southern California Current System observed by underwater gliders. Geophys. Res. Lett. 43, 1241–1248. https://doi.org/10.1002/2015GL067550.
- Zhang, J., Kobert, K., Flouri, T., Stamatakis, A., 2014. PEAR: a fast and accurate Illumina Paired-End reAd mergeR. Bioinformatics 30, 614–620. https://doi.org/10.1093/ bioinformatics/btt593.